ORIGINAL ARTICLE
Pediatric/Craniofacial

Topological Analysis for Arteriovenous Malformations via Computed Tomography Angiography: Part 2: Practical Application

Yuki Hata, MD*
Keigo Osuga, MD, PhD†
Shuichiro Uehara, MD, PhD‡
Kenji Yano, MD, PhD*
Mamoru Kikuchi, MD, PhD*
Koichi Tomita, MD, PhD*
Ken Matsuda, MD, PhD*
Tateki Kubo, MD, PhD*
Takashi Fujiwara, MD*
Ko Hosokawa, MD, PhD*

Background: In a previous study, the authors outlined a technique for calculating the number of abnormal vascular loop structures described in 3-dimensional computed tomography angiography. To be developed into a quantitative evaluation method for soft-tissue arteriovenous malformations (AVMs), the concept needs assessment of validity.

Methods: Computed tomography angiography results of 19 soft-tissue AVMs and 18 control abdominal vessels are utilized. Enhanced vascular lumen regions over 120 HU were extracted by a region growing method and skeletonized into wire frame graph models. The number of vascular loop structures in graphs is calculated as 1 − [Number of nodes] + [Number of edges], and results are compared between AVM/control groups, pre-/postprogression, and pre-/posttreatment.

Results: Average vascular lumen capacity of AVMs was 57.5 ml/lesion, and average number of vascular loops was 548 loops/lesion. Loop density of AVMs (weighted average, 9.5 loops/ml) exhibited statistically significant ($P < 0.001$) greater value than normal abdominal blood vessels (weighted average, 1.3 loops/ml). In all 4 cases without treatment, number of loops and loop density both increased. Particularly, number of loops increased greatly by 2 times or more in 3 cases. In all 7 cases with treatment, number of loops and vascular lumen capacity significantly ($P = 0.0156$) decreased. Particularly, number of loops showed clearer decrease in cases with entire lesion treatment than partial treatment.

Conclusions: Total number of described vascular loop structures and their density or volume well reflected the existence, progression, and remission of soft-tissue AVMs. Topological analysis can be expected to be developed into a quantitative evaluation for AVMs. *(Plast Reconstr Surg Glob Open 2014;2:e207; doi: 10.1097/GOX.0000000000000151; Published online 4 September 2014.)*

Soft-tissue arteriovenous malformations (AVMs), which are the representative high-flow vascular malformations, cause various different types of vascular abnormalities and clinical symptoms, depending on their site and extent. It remains difficult to discern the degree of AVM progression quantitatively and to formulate treatment plans.

The nature of AVM pathology is the multiple occurrences of abnormal connections between arteries and veins. The authors predicted that the number of arteriovenous shunts is most directly related to the progression and improvement of the condition and used 2 mathematical concepts, namely topology and graph theory, to outline a technique for calculating the total number of described vascular loop

structures from 3-dimensional (3D) imaging data in a previous study about the mathematical concept of the topological analysis.[1]

With the objective of applying topological analysis to practice, this study aimed to verify whether the number of detected vascular loops in AVMs is more than that of normal vessels, whether the number increased without medical intervention, and whether treatment led to a decrease in the number of vascular loops in AVMs. It is anticipated that if these objectives can be fulfilled, determination of loop number by imaging could be developed into a reliable index for evaluating the degree of AVM progression and therapeutic effects.

PATIENTS AND METHODS

Patient Population

The study protocol was approved by the Institutional Review Board at Osaka University Hospital (Osaka, Japan), and written informed consent was obtained from all patients. A retrospective study was conducted on the results of computed tomography angiography (CTA) from AVM patients who were seen on an outpatient basis at the Department of Plastic Surgery, Osaka University Hospital between January 2010 and January 2013. A total of 19 cases (11 men and 8 women; mean age, 34.3 years; range, 8–71 years) were targeted because they met the prescribed imaging conditions and contracted no other metabolic or circulatory underlying disease.

AVM diagnosis was performed by confirming an obvious mass of vascular loops at the site of the patient's chief complaint using color Doppler ultrasound. When patients decided to accept treatment based on the results of certain CTA imaging, treatment was conducted within 2 months of this examination. If imaging was performed to determine therapeutic effects, it was performed at least 6 months after treatment and once color Doppler ultrasound findings had stabilized. Furthermore, when patients chose monitoring over time rather than treatment, imaging was performed only if symptoms related to Schobinger staging (Table 1) worsened.

As a reference, the early phase abdominal CTA results of 18 breast cancer cases (women; mean age, 52.7 years; range, 40–75 years), where the blood vessels were examined to prepare for recon-

Table 1. Schobinger Classification of AVMs

Stage	Features
I	Cutaneous blush/warmth
II	Bruit, audible pulsations, expanding lesions
III	Pain, ulceration, bleeding, infection
IV	Cardiac failure

structive mammoplasty with deep inferior epigastric perforator flap, were targeted as control results to meet the same imaging conditions and examined within the same period as AVM patients. No patient had other metabolic or circulatory underlying disease, and 2 plastic surgeons (K.Y. and M.K.) confirmed that no anatomical abnormalities were found in the control data.

CTA Data Acquisition

A multisection helical CT scanner with 16 detector rows (GE Light Speed Ultra 16, General Electric, Milwaukee, Wisc.) was used for CTA.

In AVM cases, a bolus-tracking technique was used to synchronize the arrival of contrast in AVM with the initiation of the scan. To monitor the arrival of contrast material, axial scans were obtained at the level of proximal arteries near lesions. A contrast-enhanced scan was obtained using nonionic contrast medium (Iopamiron 300, Schering, Osaka, Japan, 300 mg iodine/ml) at a flow rate of 3 ml/s with a power injector followed by a 40-ml saline chaser. Scans were automatically triggered using monitoring software to identify a rise of 100 HU in the proximal vascular segment. The standard contrast dose was 2 ml/kg body weight, and in cases with large lesions, contrast medium volume was regulated as appropriate to contrast the entire lesion. The scan parameters were as follows: detector collimation, 0.625 mm; gantry rotation period, 0.5 second; tube voltage, 120 kV; and the tube current ranged from 150 to 440 mA according to automatic modulation depending on scanned part size.

Images were reconstructed to 16-bit grayscale 512×512 pixel images with a standardized protocol with the same section thickness (0.625 mm) and similar field of view (head and neck, 180–280 mm; trunk, 320–345 mm; extremity, 140–240 mm). When conducting multiple tests on the same patient, a particular effort was taken to maintain the same imaging conditions for each test.

In control cases, scan parameters were as follows: detector collimation, 0.625 mm; tube voltage, 120 kV; field of view, 320–345 mm; and the bolus-tracking technique using the nonionic contrast medium and automatic tube current modulation same as AVM cases was used.

Vascular Lumen Identification

The DICOM image stacks acquired through imaging were processed using OxiriX version 5.5.2 (OxiriX foundation, Geneva, Switzerland) open source medical imaging processing software[2] on a regular MacOS X (Apple, Inc., Cupertino, CA) home computer.

At first, only the bony regions were eliminated using the bone removal function while confirming the volume rendering 3D images. Next, continuous regions rendered from CT values over 120 HU were considered contrast medium and extracted en masse by the region growing method and using the feeding artery origin as the starting point in AVM cases (Fig. 1A). By doing this, the vascular lumen of only the lesion area is rendered as a continuous, single area.

When using test results obtained at different times from the same patient, care was taken to use image stacks of the same number of slices with fixed points such as junctions of well-known blood vessels and feeding arteries as reference points so that the region of interest was maintained constant. In control cases, enhanced vessels from the level of renal artery to lateral circumflex femoral artery were cropped (Fig. 2)

Binarize

Thereafter, data were processed using ImageJ version 1.46 (National Institutes of Health, Bethesda, Md.) open source image processing software[3] and the BoneJ version 1.3.9 plug-in.[4] Rendered areas were binarized into monochrome images with the command "Make Binary," and the vascular lumen was converted into a 3D structure with clearly defined borders (Fig. 1B)

Purify

Next, topological noise was reduced by filling in the enclosed spaces in the 3D structure using the "Purify" command.[5] As no other soft tissue was suspended in the vascular lumen, these enclosed spaces signified thrombus or blood that did not contain any contrast medium. We calculated

$$\left[\text{Vascular lumen capacity (ml)}\right] = \frac{[\text{BV}]}{1000}$$

on the basis of [Bone Volume (BV)] (mm³) calculated with the [Volume fraction] command.

Skeletonize

With the [Skeletonize 3D] command,[6] the thickness of all trabeculae in the 3D structure was converged into 1 voxel (volumetric pixel; Fig. 1C), and the 3D structure was simplified into a wire frame–shaped model while preserving data regarding vascular continuity.
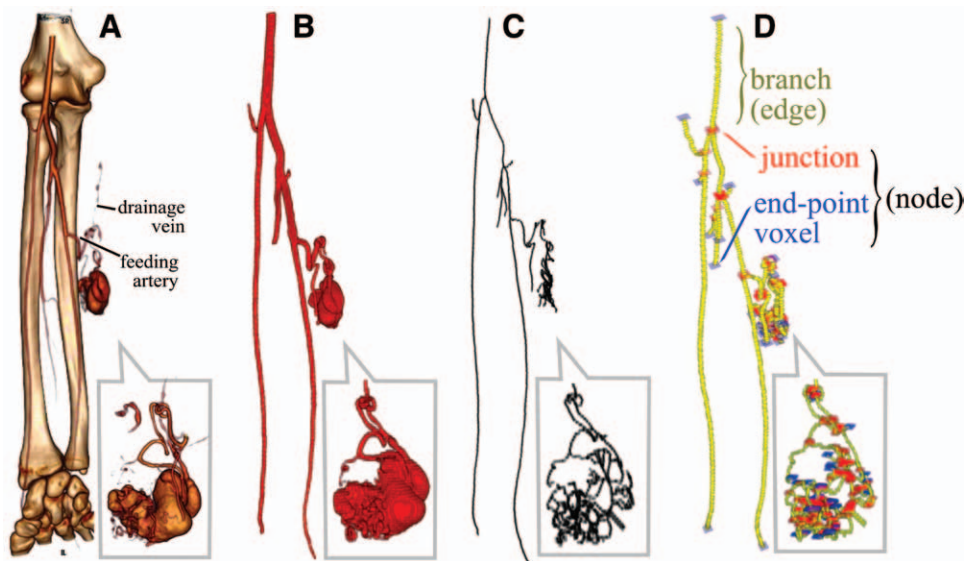
Fig. 1. Workflow images of topological analysis in a sample case (case 10: 15 years old, female, right forearm AVM). Gray squares indicate AVM lesion areas. A, Volume rendering 3D image of early phase CTA. Continuous regions rendered from CT values over 120 HU were extracted en masse by the region growing method and using the feeding artery origin as the starting point of the AVM lesion area. B, Rendered areas were binarized, the vascular lumen was converted into a 3D structure with clearly defined borders, and topological noise was reduced by filling in the enclosed spaces in the 3D structure. C, The thickness of all trabeculae in the structure was converged into 1 voxel (volumetric pixel). The vascular structure was simplified into a wire frame–shaped model while preserving its connectivity. D, The wire frame–shaped structure is considered as a graph, and the junction voxels/end-point voxels/branches are tagged and numbered.
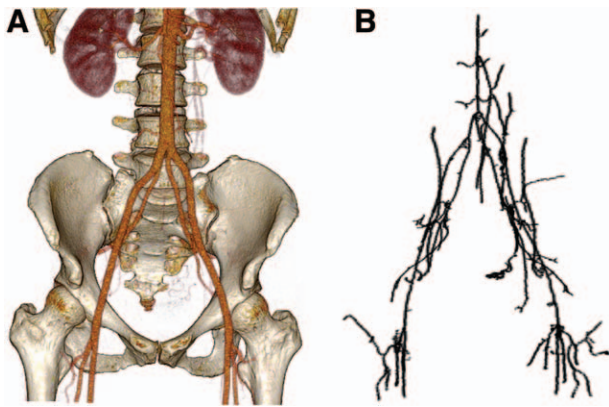
Fig. 2. Representative normal vascular image of control cases (43 years old, female, right breast cancer). A, Enhanced vessels from the level of renal artery to lateral circumflex femoral artery were cropped. B, Skeletonized vascular model shows tree-like structure consisting of internal iliac artery, inferior epigastric artery, lateral circumflex femoral artery, and their branches.

Measurement

The [Analyze Skeleton] command[7] was used on the created model. If the wire frame–shaped vascular structure is considered as a graph (Fig. 1D), the measured values can be used to express it as follows: [Number of nodes] = [Number of junctions] + [Number of end-point voxels] [Number of edges] = [Number of branches]

By substituting these into the equation outlined in a previous study about the mathematical concept of the topological analysis[1]:

$$[\text{Number of vascular loops}]$$
$$=1-[\text{Number of nodes}]+[\text{Number of edges}]$$

we calculated the following: [Number of vascular loops] = 1 − [Number of junctions] − [Number of end-point voxels] + [Number of branches]. The number of vascular loops per vascular lumen unit volume was defined as "loop density", and we then calculated the following:

$$[\text{Loop density}] = \frac{[\text{Number of vascular loops}]}{[\text{Vascular lumen capacity (ml)}]}$$

Statistical Analysis

To evaluate the difference between normal and AVM vessel structure, the Mann–Whitney U test was applied to loop density of control group and initial examination of AVM group. To evaluate the topological transformation caused by medical intervention, the Wilcoxon signed-rank test was applied to result of vascular lumen capacity, number of loops, and loop density in both pre- and postprocedural examination.

All statistical analyses were performed using statistical software (IBM SPSS Statistics version 19, IBM, Armonk, N.Y.), and a P value <0.05 was considered to indicate a statistically significant difference.

RESULTS

Clinical Findings at Initial Examination

Each AVM patient had 1 lesion site, and all cases were Schobinger stage II or III (Table 2).

Different clinical symptoms were observed at each lesion site. Of the 4 craniocervical cases (cases 1–4), hemorrhage occurred in 3 cases in which progression was noted. However, no cases were accompanied by pain or ulceration of the skin.

The 4 trunk cases (cases 5–8) experienced even fewer symptoms than the craniocervical cases, and 3 cases were classified as Schobinger stage II. Case 5 was the only exception, developing a congested skin ulcer and pulsatile bleeding in the region of the shoulder joint. However, this developed over the shoulder amputation stump that remained after the patient underwent shoulder disarticulation as a child for AVM in the arm. Therefore, this case was similar to a case of AVM of the limbs.

Of the 11 limb cases, the 2 cases proximal to the wrist or ankle (cases 9 and 10) exhibited few symptoms, similar to the trunk cases. However, 6 of the 9 cases distal to the wrist or ankle (cases 11–19) were accompanied by pain due to abnormal circulation. Different phenomenon was observed in the 2 cases (cases 15 and 19) complicated by tissue injury, such as ischemic necrosis of the finger and a stasis ulcer of the foot.

Topological Findings at Initial Examination

Vascular capacity at the initial examination varied from undersized to extremely oversized, ranging from 4.2 ml per lesion (case 13) to 387.0 ml per lesion (case 1). Mean capacity was 57.5 ml.
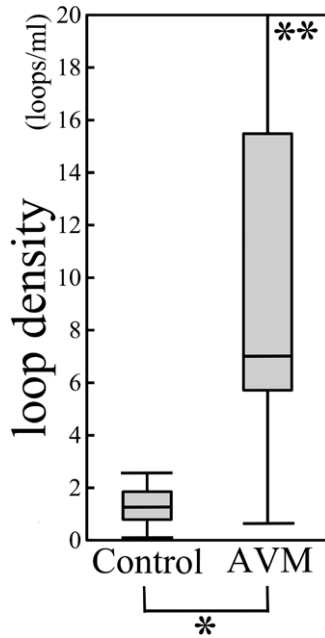
The number of loops varied from few to extremely numerous, ranging from 13 loops (case 7) to 2634 loops per lesion (case 1). Results for mean values per site with relatively similar resolutions were calculated as 893 loops in the craniocervical region, 197 loops in the trunk region, and 550 loops in the limbs.

Loop density varied according to characteristics, ranging from 0.6 loops/ml (case 7), which was a relatively low-flow cystic lesion, to extreme complexity (case 13), including 113.2 loops/ml. Their weighted average was 9.5 loops/ml, and when compared with loop density indicated by reference CTA data of normal abdominal blood vessels (weighted average, 1.3 loops/ml), AVM lesions exhibited statistically significant greater value ($P < 0.001$) (Fig. 3).

Table 2. Clinical Symptoms and Procedures and CTA Imaging Conditions of AVM Cases

Case No.	Age	Sex	Location		Bleeding	Persistent Pain	Ulceration/ Necrosis	Schobinger Staging	Vascular Lumen Capacity, ml	No. Loops	Loop Density, loops/ml	FOV, mm
1	20	M	Face and scalp	Initial visit	+	−	−	III	387.0	2634	6.8	280
2	38	M	Upper eyelid	Initial visit	−	−	−	II	16.6	467	28.1	230
				10 mo Post partial ablation	−	−	−	II	12.7	277	21.8	
3	50	M	Nose tip	Initial visit	−	−	−	II	8.2	95	11.5	240
				18 mo Untreated	+	−	−	III	6.6	188	28.3	
4	8	M	Buccal region	Initial visit	+	−	−	III	34.2	374	10.9	180
				16 mo Postembolization	−	−	−	II	23.2	58	2.5	
5	71	M	Shoulder	Initial visit	+	−	+	III	52.7	304	5.8	320
				6 mo Post total ablation	−	−	−	II	24.3	75	3.1	
6	32	M	Thoracic wall	Initial visit	−	−	−	II	9.0	91	10.1	345
7	26	F	Thoracic wall	Initial visit	−	−	−	II	20.1	13	0.6	345
				6 mo Post total resection	−	−	−	II	8.7	2	0.2	
8	32	F	Buttock	Initial visit	−	−	−	II	167.4	381	2.3	345
9	30	M	Brachium	Initial visit	−	−	−	II	70.7	332	4.7	200
				9 mo Untreated	−	−	−	II	112.0	778	6.9	
				6 mo Post partial resection	−	−	−	II	24.6	299	12.1	
10	15	F	Forearm	Initial visit	−	−	−	II	6.8	40	5.9	140
				6 mo Post total resection	−	−	−	II	3.6	1	0.3	
11	56	F	Hand	Initial visit	−	+	−	III	15.3	298	19.5	150
12	32	F	Hand	Initial visit	−	−	−	II	15.7	867	55.4	150
13	35	F	Hand	Initial visit	−	+	−	III	16.1	1819	113.2	140
14	61	F	Hand	Initial visit	−	+	−	III	4.2	27	6.4	170
15	43	M	Hand	Initial visit	+	+	+	III	57.1	321	5.6	140
16	45	M	Hand	Initial visit	−	−	−	II	35.2	101	2.9	170
				24 mo Untreated	−	+	−	III	56.4	216	3.8	
17	20	M	Hand	Initial visit	+	−	−	II	51.6	351	6.8	140
				8 mo Untreated	−	−	−	III	54.5	525	9.6	
				12 mo Post total ablations	−	−	−	II	44.1	47	1.1	
18	20	M	Foot	Initial visit	−	−	−	II	80.6	882	10.9	240
19	18	F	Foot	Initial visit	+	+	+	III	44.7	1012	22.7	220

F indicates female; FOV, field of view; M, male.

Fig. 3. Loop density comparison of 18 control abdominal vessel data and 19 AVM lesion data. Lines indicate maximum, mean, minimum; and box indicates first to third quartiles.*Statistically significant ($P < 0.001$) in the Mann–Whitney U test. **Extra outliers (55 and 113 loops/ml).
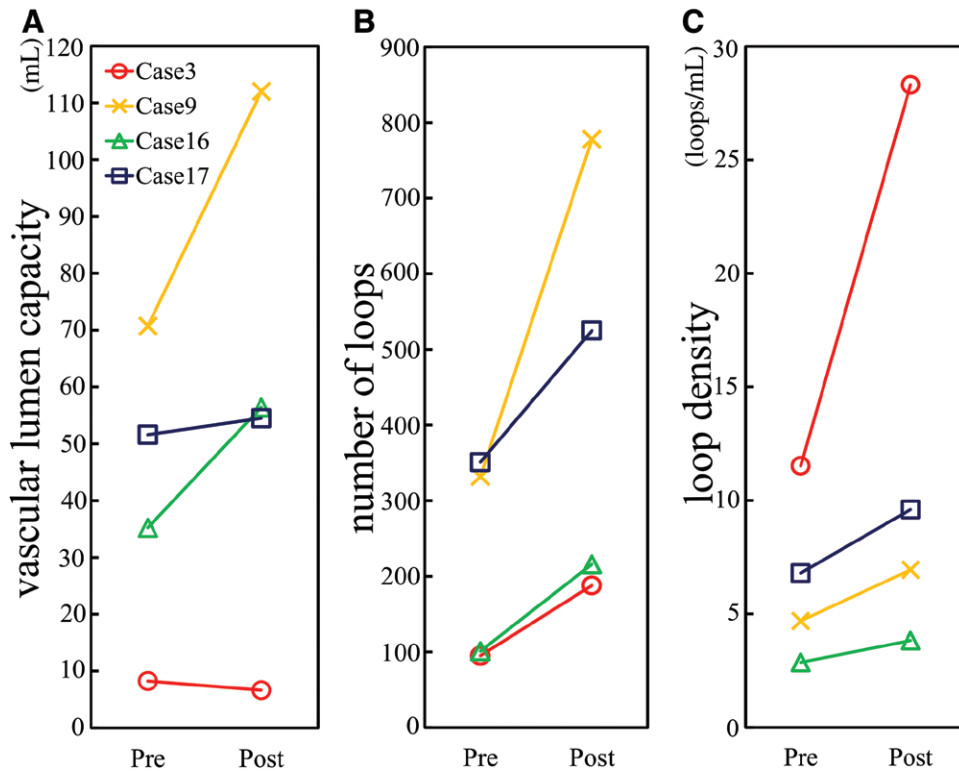
When estimated for each site, the weighted average of loop density indicated particularly low in the trunk region, with 3.2 loops/ml compared with 8.0 loops/ml in the craniocervical region and 15.2 loops/ml in the limbs.

**Topological Changes According to Progression**

Symptomatic exacerbation in the absence of treatment was evaluated in 4 cases (cases 3, 9, 16, and 17).

Measured values revealed that 8–24 months of no treatment caused lesion vascular capacity to obviously increase by approximately 1.5 times in half of the cases (case 9 and 16), whereas lesion vascular capacity showed almost no change or 20% decrease in other cases (cases 3 and 17) (Fig. 4A).

Although the number of cases was not enough for statistical verification, loop number and density both increased in all cases without treatment (Figs. 4B, C). In particular, the loop number increased greatly by 2 times or more in 3 cases (cases 3, 9, and 16). Meanwhile, the rate of changes in loop density became dull compared with that of loop number because of increased vascular lumen capacity in cases 9 and 16.

Fig. 4. Topological changes according to progression (cases 3, 9, 16, 17). Statistical verification test was not applied because of insufficient number of cases. A, The lesion vascular capacity decreased in all cases except case 3 (underwent sutures for hemostasis). B, Total loop number clearly increased in all cases without treatment. C, Loop density increased in all cases, but vascular lumen expansion made changes dull in cases 9 and 16.
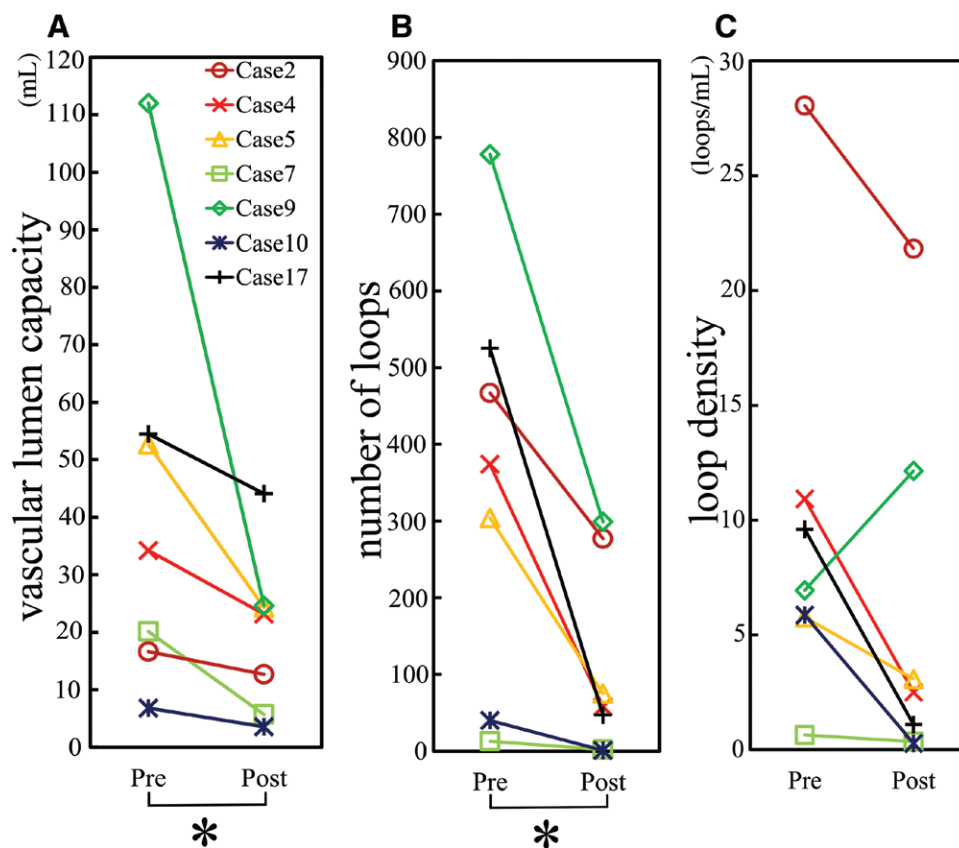
Fig. 5. Topological changes caused by treatment (cases 2, 4, 5, 7, 9, 10, 17). *Statistically significant ($P = 0.0156$). A, Vascular lumen capacity in the lesion area significantly decreased in all cases. B, Number of loops significantly decreased in all cases. The decrease was clear in the total treatment cases (cases 4, 5, 7, 10, 17) and dull in the partial treatment cases (cases 2 and 9). C, Changes in loop density differed according to the scale of treatment. Clear decrease was noted in entire treatment cases (cases 4, 5, 7, 10, 17), and the values barely changed in partial treatment cases (cases 2 and 9).

Topological Changes Caused by Treatment

Therapeutic effects were evaluated in 7 cases (cases 2, 4, 5, 7, 9, 10, and 17).

Surgical resection was performed in cases 7, 9, and 10; however, the resection range was limited within subcutaneous tissue to preserve biceps brachii muscle in case 9 (partial resection). Cicatrization using radiofrequency ablation[8] as a preparation for resection was performed in cases 2, 5, and 17; however, the ablation range was limited within subcutaneous tissue to preserve the levator palpebrae superioris muscle in case 2 (partial ablation). In case 4, endovascular embolization with n-butyl cyanoacrylate was performed.

Regardless of the type of treatment conducted, vascular lumen capacity in the lesion area decreased in all cases to 28%–81% compared with previous values (Fig. 5A), and that change was statistically significant ($P = 0.0156$).

The number of loops also decreased in all cases because of treatment (Fig. 5B), and statistical significance was indicated ($P = 0.0156$). However, the strength of therapeutic effects differed according to the scale of treatment, with 75%–98% loops disappearing in the total resection/ablation/embolization cases (cases 4, 5, 7, 10, and 17), whereas only 41%–64% disappeared in the partial resection/ablation cases (cases 2 and 9).

The scale of treatment also influenced changes in loop density (Fig. 5C). Although a clear decrease was noted in the 5 cases (cases 4, 5, 7, 10, and 17) where treatment targeted the entire lesion and an approximately 95% decrease was observed in case 10, the values barely changed in the 2 cases that underwent partial treatment (cases 2 and 9). Furthermore, records showed that in case 9, loop density exhibited a temporary postoperative increase of approximately 2.5 times compared with preoperative data.

DISCUSSION

Significance of Each Parameter

Our analysis indicated that AVMs have denser vascular loops than normal vessels, and their progres-
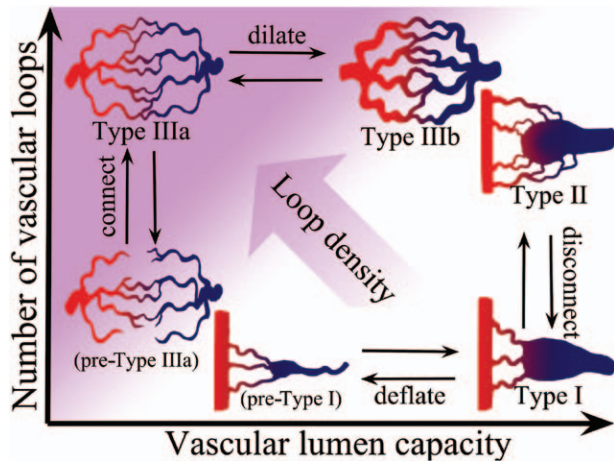
Fig. 6. Mutual transition between various types of AVMs are expected from a geometrical viewpoint. Classification by Cho et al.[10] Types I and II are considered to be a close relation differentiated by their connectivity. Types IIIa and IIIb are considered to be a close relation differentiated by their vascular diameter. Type I with lower vascular lumen capacity (as it were pre–type I) and type IIIa with fewer vascular connections (as it were pre–Type IIIa) are similar to normal vessel structures and sometimes overlooked as subclinical AVMs. Type I sometimes shows lower loop density than normal.

Fig. 7. Detailed course, 3D CTA images, and their AVM morphology (classification by Cho et al[10]) of case 9 (30 years old, male, left brachial AVM). At initial examination and 9 months untreated, the AVM morphology was type II, which contains dilated venous cavity. Six months after surgery, the volume of the lesion had greatly decreased due to resection of nidus which mainly consists of a dilated venous cavity, and remaining plexiform arteriolovenulous shunts (type IIIa) caused a temporary increase in loop density. Twelve months after surgery, excessive microscopic shunts regressed without having much effect on vascular lumen capacity, reducing loop density. But a lesion with smaller scale and unchanged loop density from the initial examination is persistent in the end.
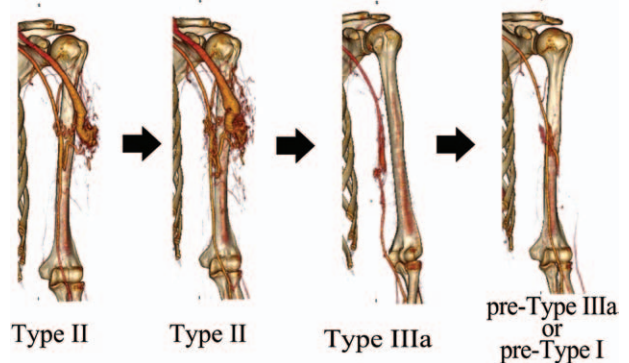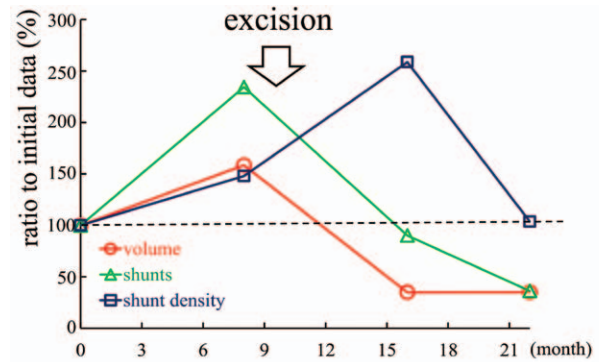
sion is accompanied by an increase in the number and density of vascular loops contained within the lesion. However, increase in loop density itself does not necessarily reflect the progression of the lesion. Loop density is only indicative of lesion shape.

Even in lesions with the same number of loops, high loop density indicates a lesion with diffuse microscopic arteriovenous fistulas and percutaneous/transcatheter interventional radiology is likely to be difficult. In contrast, low loop density represents a tortuous feeding artery or an abundance of cavities in a dilated arterialized vein and is indicative of a high risk for hemorrhage if surgery is conducted.[9,10] Dynamically, increased loop density signifies that "the lesion has increased its internal connections or has deflated." In contrast, decreased loop density signifies that "the lesion has decreased its internal connections or has expanded" (Fig. 6).

Applicability to Prediction of Course

Of all the treatment cases, case 9 provided most data regarding morphological changes in the lesions over the course of treatment (Fig. 7). The AVM morphology in this case was type II according to the classification by Cho et al,[10] and the proportion in the dilated venous cavity side of the extracted lesion increased.

Therefore, although the volume of the lesion had greatly decreased 6 months postoperatively, transition to type IIIa plexiform arteriolovenulous shunts remaining in the area may have caused a temporary increase in loop density. Data at 12 months after

surgery showed that excessive microscopic shunts regressed without having much effect on vascular capacity, reducing loop density.

Despite this, because the loop density (lesion shape) itself is approximately the same as at the time of the initial examination, we can be cautioned that the results of this surgery are only about the same as palliation to arteriovenous fistula–like, as it were pre–type IIIa or pre–type I state, and in fact, this brachial AVM relapsed 1 year later from the last CTA inspection.

Mathematical analysis was useful for evaluating the risk of relapse in this instance, as the case continually exhibited few symptoms and remained at Schobinger stage II over the course of its development, whereas on CTA images, it appeared that the lesion had gone into remission macroscopically.

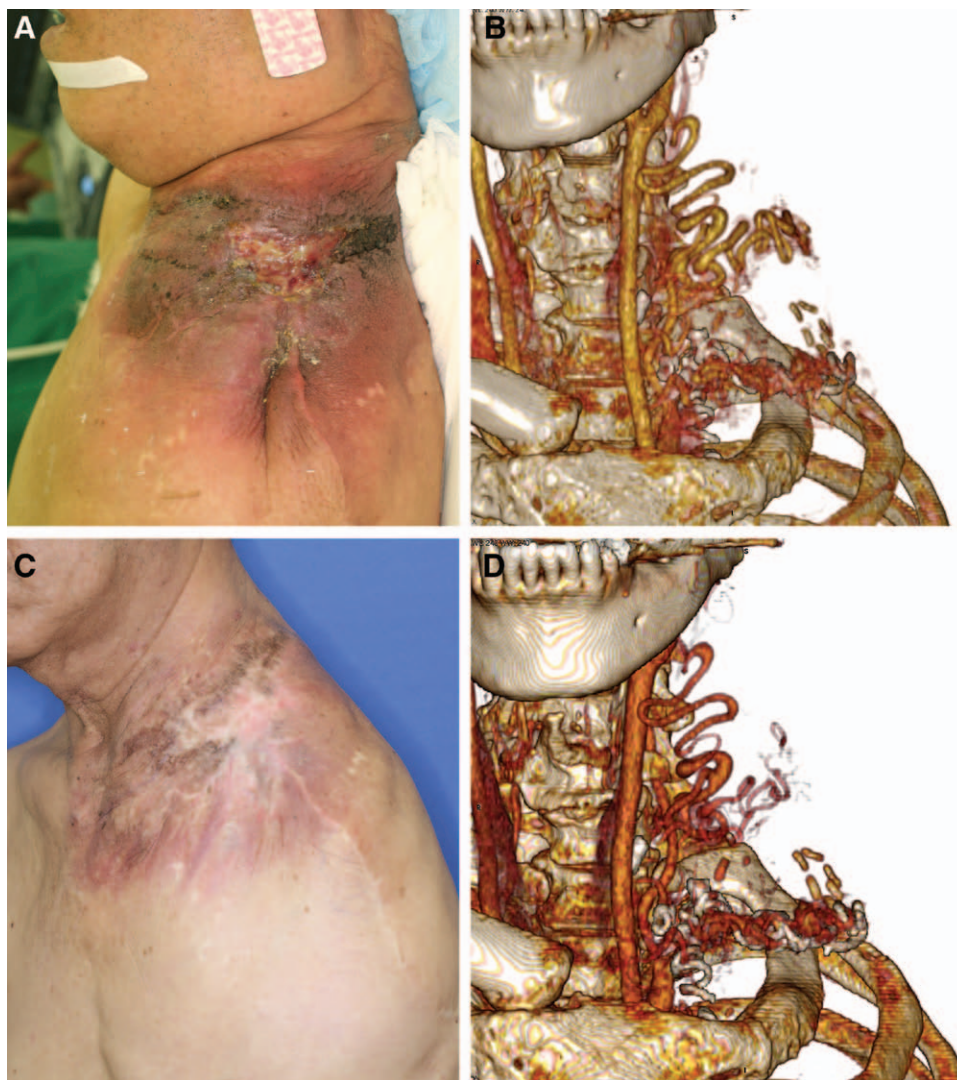In contrast, although symptoms of case 5 disappeared dramatically with treatment, changes in

vascular structure could not be discerned macroscopically from CTA images (Fig. 8).

However, the decreased vascular capacity, loop number, and loop density indicated by mathematical analysis depict the fact that the blood vessel of the lesion in this patient developed from a thick abnormal mesh into a thin normal tree, and in fact, no relapse of this shoulder AVM has been observed at the present moment of 3 years after surgery.

CONCLUSIONS

In conclusion, although this was a pilot study with a limited number of cases, application of topological analysis showed that the density of vascular loop structures in AVMs was more than that of normal vessels, and a lack of treatment in the same patient led to an increase in the number of loops, whereas treatment led to a decrease in the number. As symptoms and CTA imaging conditions for AVMs vary according to the site, this technique needs to be refined and standardized to obtain more testing data, which could be used for a better prediction of the course of AVMs. Our analysis is a technique that can be practiced immediately and cheaply by any clinician with a combination of already commonly used CT equipment, a low-end personal computer, and multiplatform open source softwares. Because AVMs can exist beyond the soft tissues, including the brain, lungs,

Fig. 8. Case 5 (71 years old, male, left shoulder AVM): a representative case in which changes in vascular structure could not be discerned macroscopically, despite symptoms disappeared dramatically with treatment and topological analysis showed normalization of vascular structure. A and B, Preoperative condition and 3D CTA image. The patient was having chronic ulceration and abrupt pulsatile bleeding during sleep. C and D, Six months postoperation. The chronic ulcer has totally epithelized. Macroscopically, changes in vascular structure could not be discerned from CTA.

and intraperitoneal organs, this technique can be broadly tested by other clinical departments.

Yuki Hata, MD
Department of Plastic Surgery
Osaka University Graduate School of Medicine
Osaka, Japan
E-mail: yukihata@gmail.com

REFERENCES

1. Hata Y, Osuga K, Kubo T, et al. Topological analysis for arteriovenous malformations via computed tomography angiography part 1: mathematical concepts. *PRS Glob Open.* 2014. doi: 10.1097/GOX.0000000000000163.
2. Rosset A, Spadola L, Ratib O. OsiriX: an open-source software for navigating in multidimensional DICOM images. *J Digit Imaging.* 2004;17:205–216.
3. Schneider CA, Rasband WS, Eliceiri KW. NIH Image to ImageJ: 25 years of image analysis. *Nat Methods.* 2012;9:671–675.
4. Doube M, Kłosowski MM, Arganda-Carreras I, et al. BoneJ: free and extensible bone image analysis in ImageJ. *Bone.* 2010;47:1076–1079.
5. Odgaard A, Gundersen HJ. Quantification of connectivity in cancellous bone, with special emphasis on 3-D reconstructions. *Bone.* 1993;14:173–182.
6. Lee TC, Kashyap RL, Chu CN. Building skeleton models via 3-D medial surface axis thinning algorithms. *CVGIP Graph Model Image Process.* 1994;56:462–478.
7. Arganda-Carreras I, Fernández-González R, Muñoz-Barrutia A, et al. 3D reconstruction of histological sections: application to mammary gland tissue. *Microsc Res Tech.* 2010;73:1019–1029.
8. van der Linden E, Overbosch J, Kroft LJ. Radiofrequency ablation for treatment of symptomatic low-flow vascular malformations after previous unsuccessful therapy. *J Vasc Interv Radiol.* 2005;16:747–750.
9. Bo Park K, Soo Do Y, Kim D-I, et al. Predictive factors for response of peripheral arteriovenous malformations to embolization therapy: analysis of clinical data and imaging findings. *J Vasc Interv Radiol.* 2012;23: 1478–86.
10. Cho SK, Do YS, Shin SW, et al. Arteriovenous malformations of the body and extremities: analysis of therapeutic outcomes and approaches according to a modified angiographic classification. *J Endovasc Ther.* 2006;13: 527–538.